# SCIENTIFIC REPORTS

**OPEN**

# Durability Enhancement of Intermetallics Electrocatalysts via N-anchor Effect for Fuel Cells

Xiang Li[1], Li An[2], Xin Chen[3], Nanlin Zhang[2], Dingguo Xia[2], Weifeng Huang[4], Wangsheng Chu[4] & Ziyu Wu[4]

[1]R&D Centre for Vehicle Battery and Energy Storage, General Research Institute for Nonferrous Metals, Beijing 100088, China, [2]College of Engineering, Peking University, Beijing 100871, P. R. China, [3]College of Environmental and Energy Engineering, Beijing University of Technology, Beijing 100124, P. R. China, [4]University of Science and Technology of China, NSRL, Hefei 230026, P. R. China.

Insufficient durability and catalytic activity of oxygen reduction reaction (ORR) electrocatalyst are key issues that have to be solved for the practical application of low temperature fuel cell. This paper introduces a new catalyst design strategy using N-anchor to promote the corrosion resistance of electrocatalyst. The as-synthesized N-Pt$_3$Fe$_1$/C shows a high electrocatalytic activity and a superior durability towards ORR. The kinetic current density of N-Pt$_3$Fe$_1$/C as normalized by ECSA is still as high as 0.145 mA cm$^{-2}$ and only 7% loss after 20000 potential cycles from 0.6 to 1.2 V (vs. NHE) in O$_2$-bubbling perchloric acid solution, whereas Pt$_3$Fe$_1$/C shows 49% loss under the same tests. The N-anchor approach offers novel opportunities for the development of ORR catalyst with excellent electrochemical properties.

Oxygen reduction reaction (ORR) plays a key role for both metal-air batteries and low-temperature fuel cells[1–8]. The sluggish electron-transfer kinetics process demands high loading of active Pt catalyst which hinders large scale application of fuel cell because of the limited supply, high cost and finite lifetime of platinum[9–11]. To address these problems, the common method is to reduce Pt usage by alloying Pt with transition metal[12–17]. Abruna and coworkers reported that a wide range of intermetallic compounds exhibit enhanced electrocatalytic activity when compared to pure Pt[18–22]. Sun and coworkers first reported that structurally ordered PtFe is more electrocatalytic active than PtFe with chemically disordered face centered cubic structure for ORR[23,24]. However, the long-term stability of alloy catalysts, due to the second metal dissolution, particle growth and corrosion of the carbon support at high potential, remains a major challenging.

The durability of electrocatalysts appears one of the most important issues that has to be addressed before the commercialization of proton exchange membrane fuel cells[25–34]. Schuth employed the combination of highly graphitized carbon to reduce carbon corrosion and interconnected pore system in order to encapsulate Pt nanoparticles to overcome the long-term catalyst degradation[35]. Nørskov[36,37], Chorkendorff[38–40], and Yoo[41–44] teams reported a stable cathode catalysts of Pt alloyed with early transition metals. Markovic and Adzic *et al.* also demonstrated stable a cathode catalysts of Pt alloyed with a 3d transition metal[45–52]. Considerable improvements in catalytic performance have been achieved.

In this work, we present a novel approach to develop durable Pt-based intermetallic electrocatalysts towards ORR by N-anchor-metal. In addition to provide a promising electrocatalyst candidate, this work demonstrates a novel design strategy of catalyst by N-anchor-metal, which can be extended to a wide variety of durable alloy catalysts.

The supported N-containing intermetallic N-Pt$_3$Fe$_1$ nanoparticles were synthesized by a simple two-stage approach. At first, supported chemically disordered Pt$_3$Fe$_1$ nanoparticles were prepared via ultrasonic-assisted electroless deposition in a mixed solution of ethylene glycol (EG)/H$_2$O without using surfactant. Subsequently, the supported N-containing intermetallic compound N-Pt$_3$Fe$_1$ nanoparticles were obtained via annealing of the as-prepared supported chemically disordered Pt$_3$Fe$_1$ nanoparticles under NH$_3$ atmosphere at 873 K for 3 hours. To evaluate the N-anchor effect in N-Pt$_3$Fe$_1$/C, the letter were also prepared via annealing of the obtained supported chemically disordered Pt$_3$Fe$_1$ nanoparticles under 95 vol%Ar + 5 vol%H$_2$ atmosphere.

The crystal structure of products was characterized with X-ray techniques. Figure 1 shows the X-ray diffraction (XRD) patterns of as-prepared Pt$_3$Fe$_1$/C, intermetallics Pt$_3$Fe$_1$/C and N-containing intermetallics N-Pt$_3$Fe$_1$/C, respectively. The XRD pattern of the as-prepared Pt$_3$Fe$_1$/C displays the distinct faced centered cubic pattern
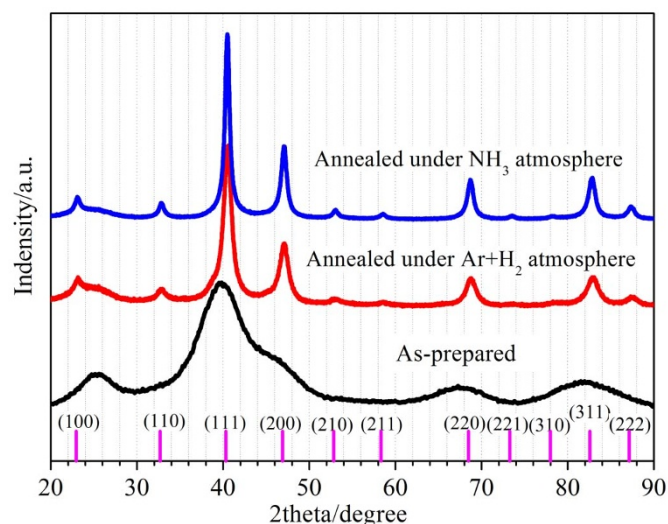
**Figure 1 | XRD patterns of as-prepared $Pt_3Fe_1$/C, intermetallics $Pt_3Fe_1$/C and N-containing intermetallics N-$Pt_3Fe_1$/C.** Vertical lines show the peak positions of chemically ordered intermetallics $Pt_3Fe_1$(JCPDS card No.89-2050).

associated to chemically disordered Pt solid solution structure. After annealed under 95 vol%Ar + 5 vol%$H_2$ atmosphere, the structure was converted from chemically disordered structure (A1 phase) to chemically ordered structure (L12 phase, space group: Pm-3m). XRD patterns of powder obtained via annealing of the as-prepared $Pt_3Fe_1$/C under $NH_3$ atmosphere suggest they have a chemically ordered $Pt_3Fe_1$ faced centered cubic structure with the Pm-3m space group, similar to powders obtained via annealing of as-prepared $Pt_3Fe_1$/C under Ar + $H_2$ atmosphere. However, the diffraction peaks of N-$Pt_3Fe_1$/C are slightly shifted to lower angles compared to those of $Pt_3Fe_1$/C (Figure S1). The observation is related to the expansion of lattice as a result of nitrogen incorporated into intermetallic $Pt_3Fe_1$ structure. The crystal structure from chemically disordered to chemically ordered during annealing is shown in figure 2. To verify the phase transformation during the annealing process, X-ray absorption spectroscopy (XAS) experiments were also performed. The results shown in figure S2 further verify the occurrence of a structural phase transition and the formation of an ordered structure (L1$_2$ phase).

Transmission electron microscopy (TEM) images of the as-prepared nanoparticles of supported chemically disordered and ordered $Pt_3Fe_1$ are shown in figure S3. The average size of as-prepared $Pt_3Fe_1$ nanoparticles was ca. 2 nm. After annealing under reductive atmosphere, the size of intermetallics $Pt_3Fe_1$ nanoparticles increased to ca. 5 nm. TEM images of supported N-containing intermetallic N-$Pt_3Fe_1$ nanoparticles are shown in figure 3. The N-containing intermetallic N-$Pt_3Fe_1$ nanoparticlse with diameters of ca.5 nm are highly dispersed on XC-72 carbon black.

Figure 4a shows N 1s X-ray photoelectron spectra (XPS) of N-$Pt_3Fe_1$/C while no N 1s signal can be collected in the intermetallic $Pt_3Fe_1$/C. The N 1s peak can be deconvoluted into three peaks. The
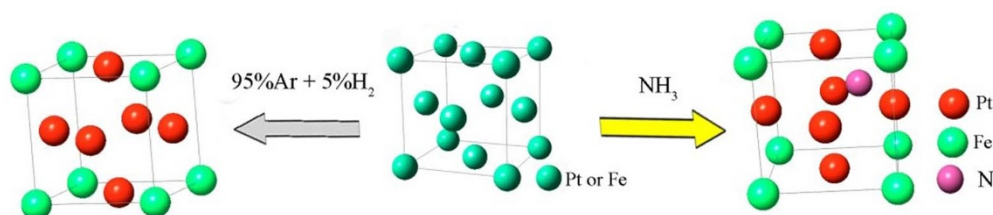
peak located in ca.398.2 eV can be assign to N which interacts with intermetallics $Pt_3Fe_1$ and the other two peaks can be assign to N which interact with oxygen species according Fairbrother's works[53]. Figure 4b and 4c show Pt 4f spectra of intermetallic $Pt_3Fe_1$/C and N-containing intermetallic N-$Pt_3Fe_1$/C, respectively. Each Pt 4f peak can be deconvoluted in two pairs of doublets. The doublet peaks of labelled 1 and 1′ are generated by photoelectrons emitted from Pt(0) while the other doublet peaks of labelled 2 and 2′ are generated by photoelectrons emitted from Pt(II). The smaller amount of Pt(II) is observed in the N-containing intermetallic N-$Pt_3Fe_1$/C. XPS spectra of Fe in the N-$Pt_3Fe_1$/C also displays an enhanced intensity of peak at low energy, suggesting a decreased contribution of the higher oxidation state Fe species(figure S4). XPS results indicate also that the introduction of nitrogen enhances the oxidation resistance of the N-$Pt_3Fe_1$. We claim it as the N-anchor effect. As to the origin of the enhanced corrosion tolerance, potentiodynamic polarization was employed to evaluate the corrosion behavior of N-$Pt_3Fe_1$/C, as shown in figure S5. The corrosion potential of the N-$Pt_3Fe_1$/C is higher than that of $Pt_3Fe_1$/C, and the corrosion current of the N-$Pt_3Fe_1$/C is lower than that of $Pt_3Fe_1$/C. That means the N-$Pt_3Fe_1$/C could show a good durability during ORR process. Furthermore, figure S2 shows the Pt L3 edge XANES spectra. The intermetallic N-$Pt_3Fe_1$/C exhibits a decreased Pt L$_3$-edge white line intensity compared to the intermetallic $Pt_3Fe_1$/C. The L$_3$ edge XANES spectroscopy at the Pt originates from the electron excitation from core 2s to 5d unoccupied state. The decrease in the white line intensity reflects the decreased number of unoccupied d-states of Pt in the N-$Pt_3Fe_1$/C catalyst, implying the high resistance to be oxidized for Pt.

Previous works showed that doping nitrogen into a carbon support by nitrogen ion beam or ammonia reaction at 1173 K significantly impedes Pt nanoparticles migration and coarsening[54–57]. In this work, to investigate the interaction of $NH_3$ with the support of XC-72 at 873 K, we measured C1s XPS spectra of as-prepared $Pt_3Fe_1$/C, intermetallic $Pt_3Fe_1$/C and N-containing intermetallic N-$Pt_3Fe_1$/C, as shown in figure 4d. It clearly shows that there is no evidence of interaction between nitrogen and carbon.

To further characterize N in N-$Pt_3Fe_1$/C, N K-edge XAS spectrum was also measured. Figure 5 compares the calculated theoretical and experimental spectra, which present four significant features marked with vertical dashed lines. Using the "fingerprint" of the N K-edge XAS, we may show that the simulated spectrum of N-$Pt_3Fe_1$ with the N atom in a tetrahedral site matches the raw spectrum.

In figure 6a we compare typical CV curves of commercial Pt/C (Johnson Matthey HiSPEC 3000), chemically ordered $Pt_3Fe_1$/C and N-$Pt_3Fe_1$/C in Ar-saturated 0.1 M $HClO_4$. All the Pt-based electrocatalysts show the region of H-adsorption and H-desorption in the potential range of 0.05 to 0.40 V, the double-layer capacitance region located from 0.40 to ca. 0.60 V and the region of Pt oxidation and Pt-oxide reduction in the range of ca. 0.60–1.20 V. The electrochemical surface area (ECSA) of the electrocatalysts has been calculated by integrating H-desorption charges, a method used to normalize the kinetic current density to evaluate the intrinsic electrocatalytic activity of Pt-based electrocatalysts. The CV curves did not show any anodic currents ascribed to the oxidation/dissolution of Fe, demonstrating that Fe is stabilized by N-anchor. The EDS line scanning
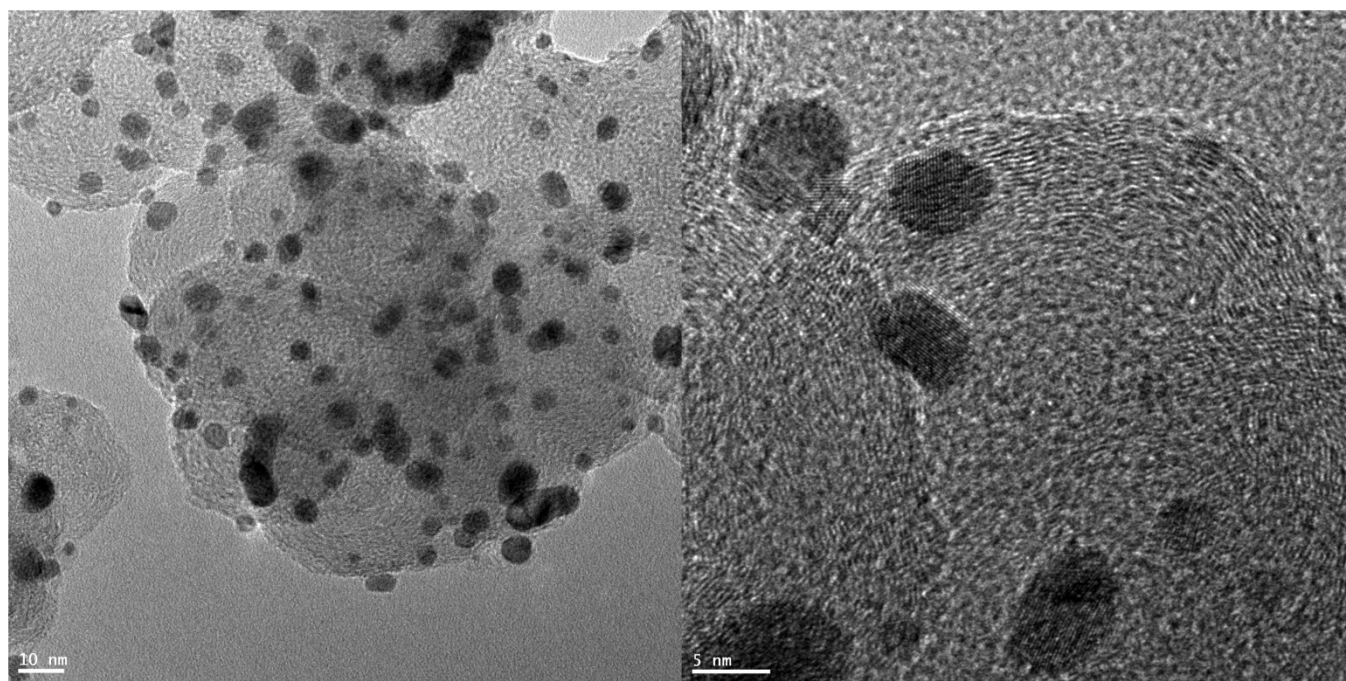


**Figure 2 | Illustration of phase transition during annealing process.**

**Figure 3** | TEM images of supported N-containing intermetallic compound N-$Pt_3Fe_1$ nanoparticles obtained at 873 K for 3 hours.
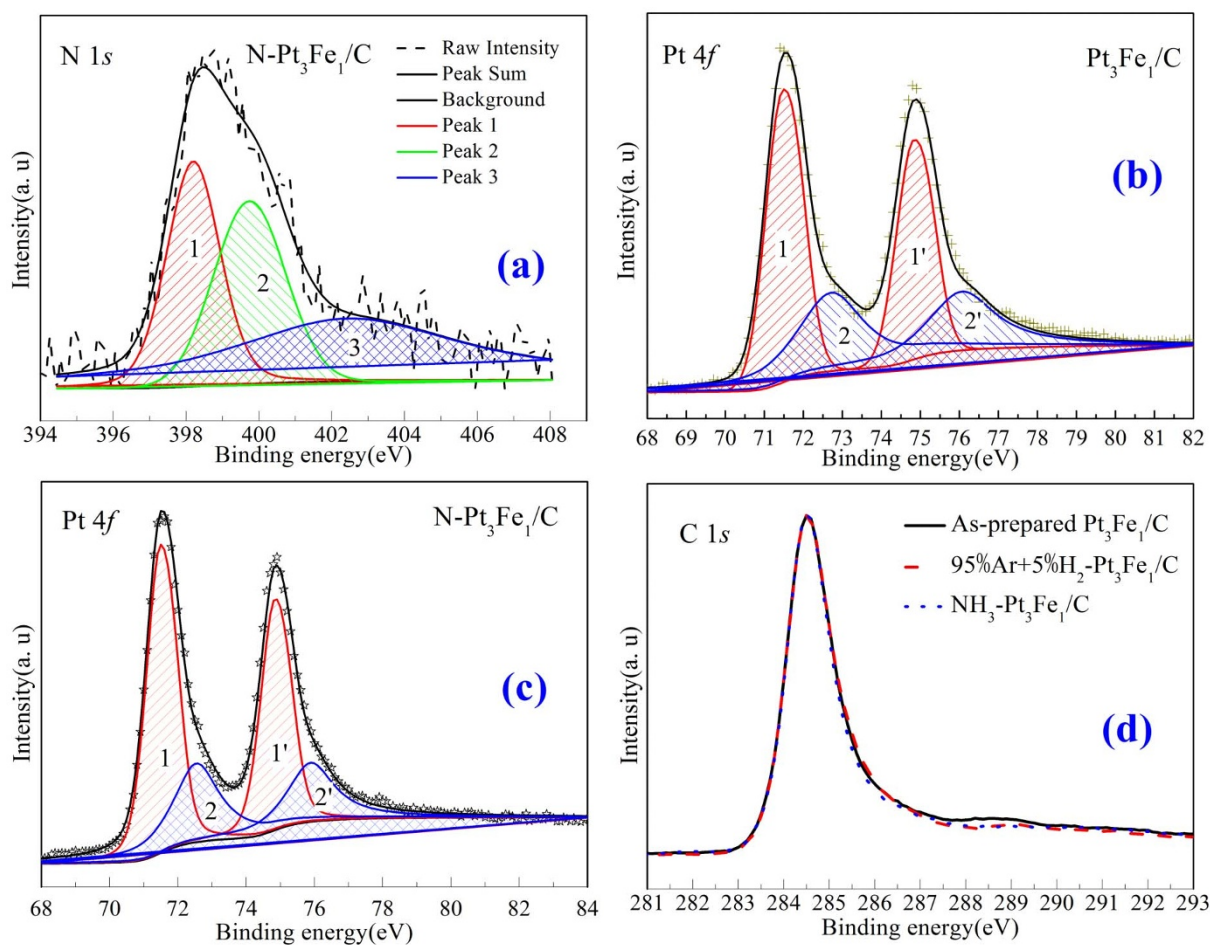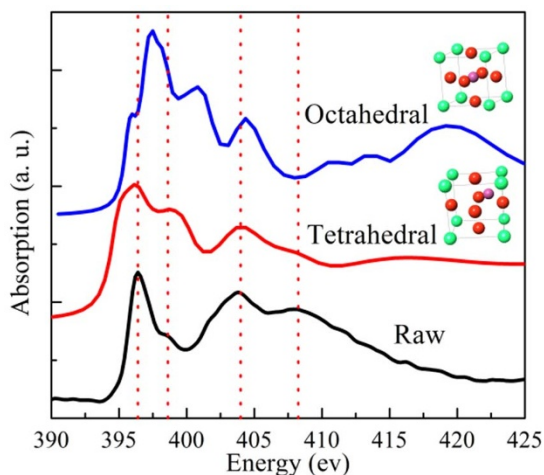


**Figure 4** | XPS spectra(a, b, c, d) of as-prepared $Pt_3Fe_1$/C(C 1s), intermetallics $Pt_3Fe_1$/C (Pt 4f and C1s) and N-containing intermetallics N-$Pt_3Fe_1$/C (Pt4f, N 1s and C1s).

**Figure 5 | Experimental N K-edge XAS spectra of N-Pt$_3$Fe$_1$/C and calculated octahedral-N-Pt$_3$Fe$_1$ and tetrahedral-N-Pt$_3$Fe$_1$.**

and mapping results, as shown in figure S6, point out that the structure of the N-Pt$_3$Fe$_1$/C nanoparticle is intact and no structural transformation after potential cycles from 0.6 to 1.2 V in O$_2$-bubbling perchloric acid solution, further witnessing the good durability of the catalyst.

The electrocatalytic activity for ORR was evaluated using rotating disk electrode in O$_2$-saturated 0.1 M HClO$_4$ at room temperature. In order to compare the specific activity for different electrocatalysts according to the Levich-Koutecky equation, the kinetic current was calculated from the polarization curve (Figure S7) by considering the mass-transport correction and normalized with respect to electrochemical active surface area. Both Pt$_3$Fe$_1$/C and N-Pt$_3$Fe$_1$/C show a higher activity towards ORR than that of the commercial Pt/C at the potential of 0.9 V. Their enhanced activities were due to their chemically ordered Pt$_3$Fe$_1$ intermetallic compound structure[17,23]. Accelerated durability tests (ADT) were performed by cycling the potential between 0.6–1.2 V (vs. NHE) in O$_2$-bubbling 0.1 M HClO$_4$ at a scan rate of 200 mV s$^{-1}$. After ADT tests, the specific activities of electrocatalysts were recorded as shown in figure 6b. It has been shown that N-Pt$_3$Fe$_1$/C showed the best durability after 5000 cycles. The kinetic current densities at 0.9 V were only decreased ca. 7% for the N-Pt$_3$Fe$_1$/C after 20000 potential cycles, whereas the Pt$_3$Fe$_1$/C shows an activity degradation of 49%. The degradation of specific

activity of the intermetallic Pt$_3$Fe$_1$/C is mainly due to the destruction of intermetallics structure deduced by the leaching of Fe during ADT tests. We assigned the enhanced durability of N-Pt$_3$Fe$_1$/C vs. Pt$_3$Fe$_1$/C to the N-anchor effect which could promote corrosion resistance of Pt$_3$Fe$_1$ intermetallics.

This work has highlights a novel strategy to promote the durability of intermetallic Pt$_3$Fe$_1$ electrocatalyst. Supported nitrogen-containing intermetallic N-Pt$_3$Fe$_1$ electrocatalyst was synthesized via a facile two-stage approach. Actually, the N-Pt$_3$Fe$_1$/C electrocatalyst shows stability under ADT tests and only show a 7% specific activity loss after 20000 potential cycles from 0.6 to 1.2 V (vs. NHE) in O$_2$-bubbling perchloric acid solution. The superior durability of the N-Pt$_3$Fe$_1$/C is assigned to the N-anchor effect that could promote corrosion resistance of electrocatalysts. This strategy of durability and activity enhancement towards ORR could be applied to the design of other alloy electrocatalysts for fuel cells.

## Methods

**Synthesis of as-prepared Pt$_3$Fe$_1$/C.** As-prepared Pt$_3$Fe$_1$/C was synthesized by one-pot reduction of Pt and Fe inorganics in EG/H$_2$O mixed solution in an ultrasonic cleaning bath. 0.3 mmol H$_2$PtCl$_6$ 6H$_2$O and 0.1 mmol FeSO$_4$ 7H$_2$O were dissolved into 200 mL EG/H$_2$O mixed solution (EG: H$_2$O = 1 : 1 in volume ratio, containing 6 mL concentrated sulfuric acid) in a three-neck flask. 234.1 mg XC-72 was then added to the flask above, yielding Pt loadings of ca.20% in weight. After the mixed solution was vigorous stirred in the ultrasonic cleaning bath for 2 hours at room temperature, the temperature of the mixed solution was increased to 65°C, and 5 mol L$^{-1}$ NaOH solution was added to adjust pH to 11. 40 mmol sodium hypophosphite (NaH$_2$PO$_2$ H$_2$O) was then added into the mixture solution. The process of the reaction is under the protection of N$_2$. After 10 hours reaction, the obtained supported Pt-Fe nanoparticles were then filtered, washed copiously with water, and dried at 80°C overnight.

**Preparation of intermetallics Pt$_3$Fe$_1$/C.** To obtain intermetallics Pt$_3$Fe$_1$/C, as-prepared Pt$_3$Fe$_1$/C was put in a quartz tube and annealed at the temperature of 873 K for 30 min under mixture gas of 95%Ar + 5% H$_2$.

**Preparation of N-containing intermetallics N-Pt$_3$Fe$_1$/C.** To obtain N-containing intermetallics N-Pt$_3$Fe$_1$/C, as-prepared Pt$_3$Fe$_1$/C was put in a quartz tube and annealed at the temperature of 873 K for 3 hours under NH$_3$ atmosphere.

**Characterization.** The X-ray diffraction (XRD) patterns of the samples were obtained using a Bruker D8 Advance diffractometer with Cu Kα(λ=1.5405Å) radiation source (40 kV, 40 mA). The morphology, structure, and component of nanoparticles were investigated on FEI Tecnai G2 F30 field-emission transmission electron microscope (TEM) and FEI Titan G2 80–200 Probe Cs-corrector Scanning transmission electron microscope (STEM). The bulk composition of the prepared catalysts was measured using the inductively coupled plasma-atomic emission spectrometry (ICP-AES) on an IRIS Intrepid spectrometer after dissolution of the samples in aqua regia and then dilution using 1 M HCl. X-ray photoelectron spectroscopy (XPS) data were collected on an AXIS-Ultra instrument from Kratos
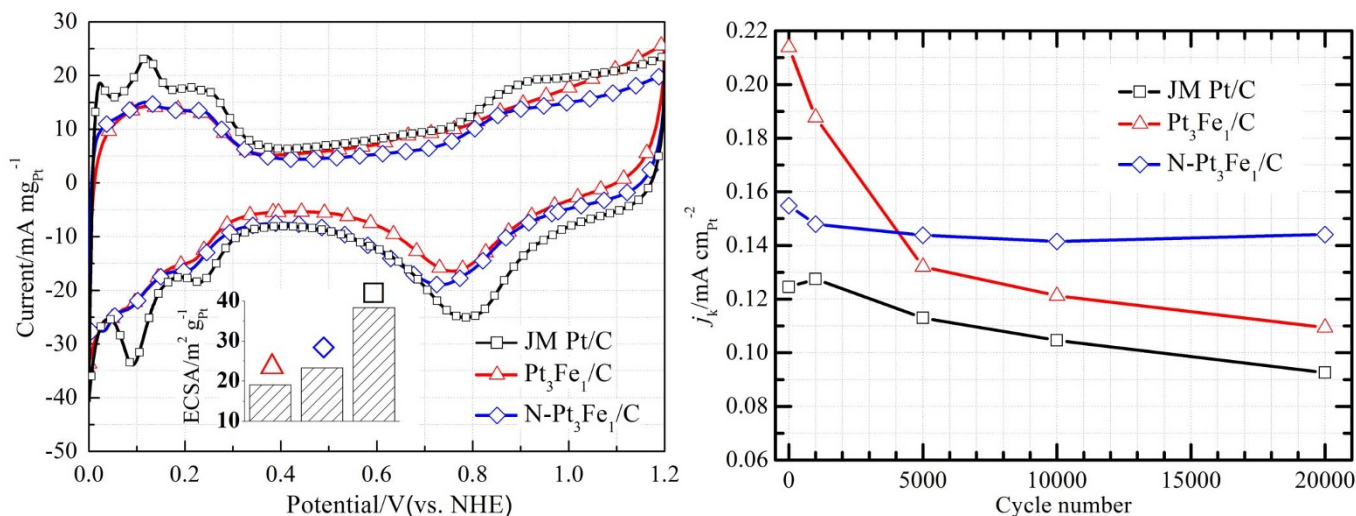


**Figure 6 |** (a) Cyclic Voltammograms and bar plots of ECSA of the commercial Pt/C, Pt$_3$Fe$_1$/C and N-Pt$_3$Fe$_1$/C. (b) plots of kinetic current density (normalized by ECSA) versus cycle number for the commercial Pt/C, Pt$_3$Fe$_1$/C and N-Pt$_3$Fe$_1$/C at 0.9 V.

Analytical using monochromatic Al Kα radiation (hν =1486.6 eV) and low-energy electron flooding for charge compensation. To compensate for the effects of surface charges, the binding energies were calibrated using the C 1s hydrocarbon peak at 284.80 eV. The Shirley method was used to correct the background of all spectra. After making the corrections, the spectra were analyzed using the XPSPEAK 4.1 software package. To deconvolute the spectra, we used a convolution of a mixed Gaussian-Lorentzian function series corrected by an asymmetric component to reflect the many-body effects in metal. Pt $L_3$-edge X-ray absorption fine structure (XAFS) spectra of intermetallics N-$Pt_3Fe_1$/C and N-containing intermetallics N-$Pt_3Fe_1$/C, as well as Pt $L_3$-edge XAFS spectrum of Pt foil as a reference compound, were measured in fluorescence mode at the Beijing Synchrotron Radiation Facility (BSRF). X-ray absorption spectra were background-subtracted and then normalized to the high energy atomic absorption. To allow comparisons to be made, the edge energy was subtracted and defined as energy zero for the Pt $L_3$-edge XANES spectra.

The electrochemical measurements were performed using a VMP3 multichannel potentiostat/galvanostat (Bio-Logic SAS, France) at a constant temperature of 25°C unless stated otherwise. The glassy carbon rotating disk electrode (GC-RDE) with an area of 0.1257 cm² was used as the working electrode. A GC film electrode and a normal hydrogen electrode (NHE) were used as the counter electrode and the reference electrode, respectively. All the potentials in this study were given on the reference of NHE. Before using a GC electrode as a substrate for the catalysts, it was polished with 0.05 μm alumina to yield a mirror finish. In order to deposit the electrocatalysts on the working electrode, we prepared the ink as follows: Typically ca. 3 mg of the electrocatalyst was dispersed in isopropyl alcohol (1 mL) together with one drop of 2% Nafion solution in an ultrasonic bath for 20 min. The suspension (10 μL) was pipetted on to the GC substrate and dried in an air oven for 30 min.

To obtain the corrosion behavior of electrocatalysts, the potentiodynamic polarization measurement was conducted in $O_2$-saturated 0.1 M $HClO_4$ solutions. Then the potential curves was obtained plotting the potential as a function of the logarithm of the current density.

Cyclic voltammetry (CV) measurements were carried out in Ar-saturated 0.1 M $HClO_4$ solutions at 50 mV s⁻¹. The electrochemical surface area (ECSA) was estimated by measuring the charge associated with hydrogen desorption (after double layer correction) between 0.05 and 0.40 V by taking the conversion factor to be 210 μC $cm_{Pt}$⁻². The ORR measurements were performed in $O_2$-saturated 0.1 M $HClO_4$ solutions using GC-RDE at a rotation of 1600 rpm and a sweep rate of 10 mV s⁻¹. The kinetic currents for ORR on GC-RDE were calculated using the Koutecky-Levich equation (1) from the ORR polarization:

$$1/j = 1/jk + 1/jd \qquad (1)$$

Where $j$ is the experimentally measured current density, $j_d$ is the diffusion limiting current density, and $j_k$ is the kinetic current density.

The ADT tests were performed in $O_2$-bubbling 0.1 M $HClO_4$ solutions by applying cyclic potential sweeps between 0.6 and 1.2 V at a sweep rate of 200 mV s⁻¹ for the given number of cycles.

1. Debe, M. K. Electrocatalyst approaches and challenges for automotive fuel cells. *Nature* **486**, 43–51 (2012).
2. Lefevre, M., Proietti, E., Jaouen, F. & Dodelet, J. P. Iron-Based Catalysts with Improved Oxygen Reduction Activity in Polymer Electrolyte Fuel Cells. *Science* **324**, 71–74 (2009).
3. Liang, Y. Y. *et al.* Co₃O₄ nanocrystals on graphene as a synergistic catalyst for oxygen reduction reaction. *Nature Mater.* **10**, 780–786 (2011).
4. Lim, B. *et al.* Pd-Pt Bimetallic Nanodendrites with High Activity for Oxygen Reduction. *Science* **324**, 1302–1305 (2009).
5. Cheng, F. Y. & Chen, J. Metal-air batteries: from oxygen reduction electrochemistry to cathode catalysts. *Chem. Soc. Rev.* **41**, 2172–2192 (2012).
6. Cao, R. G., Lee, J. S., Liu, M. L. & Cho, J. Recent Progress in Non-Precious Catalysts for Metal-Air Batteries. *Adv. Energy Mater.* **2**, 816–829 (2012).
7. Suntivich, J. *et al.* Design principles for oxygen-reduction activity on perovskite oxide catalysts for fuel cells and metal-air batteries. *Nature Chem.* **3**, 546–550 (2011).
8. Lu, Y. C. *et al.* Platinum-Gold Nanoparticles: A Highly Active Bifunctional Electrocatalyst for Rechargeable Lithium-Air Batteries. *J. Am. Chem. Soc.* **132**, 12170–12171 (2010).
9. Brouzgou, A., Song, S. Q. & Tsiakaras, P. Low and non-platinum electrocatalysts for PEMFCs: Current status, challenges and prospects. *Appl. Catal. B* **127**, 371–388 (2012).
10. Alonso-Vante, N. Platinum and Non-Platinum Nanomaterials for the Molecular Oxygen Reduction Reaction. *Chemphyschem* **11**, 2732–2744 (2010).
11. Watanabe, M., Tryk, D. A., Wakisaka, M., Yano, H. & Uchida, H. Overview of recent developments in oxygen reduction electrocatalysis. *Electrochim. Acta* **84**, 187–201 (2012).
12. Wang, C., Markovic, N. M. & Stamenkovic, V. R. Advanced Platinum Alloy Electrocatalysts for the Oxygen Reduction Reaction. *ACS Catal.* **2**, 891–898 (2012).
13. Stamenkovic, V. *et al.* Changing the activity of electrocatalysts for oxygen reduction by tuning the surface electronic structure. *Angew. Chem. Int. Ed.* **45**, 2897–2901 (2006).
14. Gasteiger, H. A., Kocha, S. S., Sompalli, B. & Wagner, F. T. Activity benchmarks and requirements for Pt, Pt-alloy, and non-Pt oxygen reduction catalysts for PEMFCs. *Appl. Catal. B* **56**, 9–35 (2005).
15. Mukerjee, S. & Srinivasan, S. Enhanced electrocatalysis of oxygen reduction on platinum alloys in proton-exchange membrane fuel-cells. *J. Electroanal. Chem.* **357**, 201–224 (1993).
16. Wang, D. S., Zhao, P. & Li, Y. D. General preparation for Pt-based alloy nanoporous nanoparticles as potential nanocatalysts. *Sci. Rep.* **1**, 5 (2011).
17. Li, X. *et al.* Supported sub-5 nm Pt–Fe intermetallic compounds for electrocatalytic application. *J. Mater. Chem.* **22**, 6047–6052 (2012).
18. Wang, D. L. *et al.* Structurally ordered intermetallic platinum-cobalt core-shell nanoparticles with enhanced activity and stability as oxygen reduction electrocatalysts. *Nature Mater.* **12**, 81–87 (2013).
19. Abe, H. *et al.* Electrocatalytic performance of fuel oxidation by Pt₃Ti nanoparticles. *J. Am. Chem. Soc.* **130**, 5452–5458 (2008).
20. Casado-Rivera, E. *et al.* Electrocatalytic oxidation of formic acid at an ordered intermetallic PtBi surface. *Chemphyschem* **4**, 193–199 (2003).
21. Casado-Rivera, E. *et al.* Electrocatalytic activity of ordered intermetallic phases for fuel cell applications. *J. Am. Chem. Soc.* **126**, 4043–4049 (2004).
22. Wang, D. L. *et al.* Tuning Oxygen Reduction Reaction Activity via Controllable Dealloying: A Model Study of Ordered Cu₃Pt/C Intermetallic Nanocatalysts. *Nano Lett.* **12**, 5230–5238 (2012).
23. Kim, J., Lee, Y. & Sun, S. H. Structurally Ordered FePt Nanoparticles and Their Enhanced Catalysis for Oxygen Reduction Reaction. *J. Am. Chem. Soc.* **132**, 4996–+ (2010).
24. Guo, S. J. & Sun, S. H. FePt Nanoparticles Assembled on Graphene as Enhanced Catalyst for Oxygen Reduction Reaction. *J. Am. Chem. Soc.* **134**, 2492–2495 (2012).
25. Borup, R. *et al.* Scientific aspects of polymer electrolyte fuel cell durability and degradation. *Chem. Rev.* **107**, 3904–3951 (2007).
26. Chen, S. G. *et al.* Nanostructured Polyaniline-Decorated Pt/C@PANI Core-Shell Catalyst with Enhanced Durability and Activity. *J. Am. Chem. Soc.* **134**, 13252–13255 (2012).
27. Yin, A. X., Min, X. Q., Zhang, Y. W. & Yan, C. H. Shape-Selective Synthesis and Facet-Dependent Enhanced Electrocatalytic Activity and Durability of Monodisperse Sub-10 nm Pt-Pd Tetrahedrons and Cubes. *J. Am. Chem. Soc.* **133**, 3816–3819 (2011).
28. Zhou, Y. K. *et al.* Enhancement of Pt and Pt-alloy fuel cell catalyst activity and durability via nitrogen-modified carbon supports. *Energy Environ. Sci.* **3**, 1437–1446 (2010).
29. Ding, L. X. *et al.* Porous Pt-Ni-P Composite Nanotube Arrays: Highly Electroactive and Durable Catalysts for Methanol Electrooxidation. *J. Am. Chem. Soc.* **134**, 5730–5733 (2012).
30. Kibsgaard, J., Gorlin, Y., Chen, Z. B. & Jaramillo, T. F. Meso-Structured Platinum Thin Films: Active and Stable Electrocatalysts for the Oxygen Reduction Reaction. *J. Am. Chem. Soc.* **134**, 7758–7765 (2012).
31. Li, Y. J. *et al.* Stabilization of High-Performance Oxygen Reduction Reaction Pt Electrocatalyst Supported on Reduced Graphene Oxide/Carbon Black Composite. *J. Am. Chem. Soc.* **134**, 12326–12329 (2012).
32. Liu, Y. & Mustain, W. E. High Stability, High Activity Pt/ITO Oxygen Reduction Electrocatalysts. *J. Am. Chem. Soc.* **135**, 530–533 (2013).
33. Ma, X. M., Meng, H., Cai, M. & Shen, P. K. Bimetallic Carbide Nanocomposite Enhanced Pt Catalyst with High Activity and Stability for the Oxygen Reduction Reaction. *J. Am. Chem. Soc.* **134**, 1954–1957 (2012).
34. Tang, L. *et al.* Electrochemical Stability of Nanometer-Scale Pt Particles in Acidic Environments. *J. Am. Chem. Soc.* **132**, 596–600 (2010).
35. Galeano, C. *et al.* Toward Highly Stable Electrocatalysts via Nanoparticle Pore Confinement. *J. Am. Chem. Soc.* **134**, 20457–20465 (2012).
36. Viswanathan, V., Hansen, H. A., Rossmeisl, J. & Norskov, J. K. Universality in Oxygen Reduction Electrocatalysis on Metal Surfaces. *ACS Catal.* **2**, 1654–1660 (2012).
37. Greeley, J. *et al.* Alloys of platinum and early transition metals as oxygen reduction electrocatalysts. *Nature Chem.* **1**, 552–556 (2009).
38. Escudero-Escribano, M. *et al.* Pt₅Gd as a Highly Active and Stable Catalyst for Oxygen Electroreduction. *J. Am. Chem. Soc.* **134**, 16476–16479 (2012).
39. Stephens, I. E. L., Bondarenko, A. S., Gronbjerg, U., Rossmeisl, J. & Chorkendorff, I. Understanding the electrocatalysis of oxygen reduction on platinum and its alloys. *Energy Environ. Sci.* **5**, 6744–6762 (2012).
40. Stephens, I. E. L., Bondarenko, A. S., Bech, L. & Chorkendorff, I. Oxygen Electroreduction Activity and X-Ray Photoelectron Spectroscopy of Platinum and Early Transition Metal Alloys. *Chemcatchem* **4**, 341–349 (2012).
41. Hwang, S. J. *et al.* Role of Electronic Perturbation in Stability and Activity of Pt-Based Alloy Nanocatalysts for Oxygen Reduction. *J. Am. Chem. Soc.* **134**, 19508–19511 (2012).
42. Hwang, S. J. *et al.* Facile synthesis of highly active and stable Pt-Ir/C electrocatalysts for oxygen reduction and liquid fuel oxidation reaction. *Chem. Commun.* **46**, 8401–8403 (2010).
43. Yoo, S. J. *et al.* Promoting effects of La for improved oxygen reduction activity and high stability of Pt on Pt-La alloy electrodes. *Energy Environ. Sci.* **5**, 7521–7525 (2012).
44. Yoo, S. J. *et al.* Enhanced stability and activity of Pt-Y alloy catalysts for electrocatalytic oxygen reduction. *Chem. Commun.* **47**, 11414–11416 (2011).

45. Stamenkovic, V. R. *et al.* Improved oxygen reduction activity on Pt₃Ni(111) via increased surface site availability. *Science* **315**, 493–497 (2007).

46. van der Vliet, D. F. *et al.* Mesostructured thin films as electrocatalysts with tunable composition and surface morphology. *Nature Mater.* **11**, 1051–1058 (2012).

47. Wang, C. *et al.* Design and Synthesis of Bimetallic Electrocatalyst with Multilayered Pt-Skin Surfaces. *J. Am. Chem. Soc.* **133**, 14396–14403 (2011).

48. Stamenkovic, V. R. *et al.* Trends in electrocatalysis on extended and nanoscale Pt-bimetallic alloy surfaces. *Nature Mater.* **6**, 241–247 (2007).

49. Kuttiyiel, K. A. *et al.* Nitride Stabilized PtNi Core-Shell Nanocatalyst for high Oxygen Reduction Activity. *Nano Lett.* **12**, 6266–6271 (2012).

50. Zhang, J., Sasaki, K., Sutter, E. & Adzic, R. R. Stabilization of platinum oxygen-reduction electrocatalysts using gold clusters. *Science* **315**, 220–222 (2007).

51. Koenigsmann, C. *et al.* Enhanced Electrocatalytic Performance of Processed, Ultrathin, Supported Pd-Pt Core-Shell Nanowire Catalysts for the Oxygen Reduction Reaction. *J. Am. Chem. Soc.* **133**, 9783–9795 (2011).

52. Wang, J. X. *et al.* Kirkendall Effect and Lattice Contraction in Nanocatalysts: A New Strategy to Enhance Sustainable Activity. *J. Am. Chem. Soc.* **133**, 13551–13557 (2011).

53. Torres, J., Perry, C. C., Bransfield, S. J. & Fairbrother, A. H. Low-temperature oxidation of nitrided iron surfaces. *J. Phys. Chem. B* **107**, 5558–5567 (2003).

54. Zhou, Y. K. *et al.* Improving PEM fuel cell catalyst activity and durability using nitrogen-doped carbon supports: observations from model Pt/HOPG systems. *J. Mater. Chem.* **19**, 7830–7838 (2009).

55. Geng, D. S. *et al.* High oxygen-reduction activity and durability of nitrogen-doped grapheme. *Energy Environ. Sci.* **4**, 760–764 (2011).

56. Li, Y. G. *et al.* An oxygen reduction electrocatalyst based on carbon nanotube-graphene complexes. *Nat. Nanotechnol.* **7**, 394–400 (2012).

57. Olson, T. S. *et al.* Enhanced Fuel Cell Catalyst Durability with Nitrogen Modified Carbon Supports. *J. Electrochem. Soc.* **160**, F389–F394 (2013).

## Acknowledgments

## Author contributions

D.X. designed the experiments. X.L., N.L.Z. and L.A. performed the experiments, and data analysis. W.H., X.C., W.C. and Z.W. conducted the calculations. D.X. and Z.W. guided the whole work and analysis. X.L. and D.X. wrote the paper.

## Additional information